Inorg. Chem. **2008**, *47*, 4005−4014

A Density Functional Theory Calculation of the Electronic Properties of Several High-Spin and Low-Spin Iron(II) Pyrazolylborate Complexes

Françoise Remacle,[†] Fernande Grandjean,[‡] and Gary J. Long*[,§]

Departments of Chemistry and Physics, University of Liège, B-4000 Sart Tilman, Belgium, and Department of Chemistry, Missouri University of Science and Technology, University of Missouri, Rolla, Missouri 65409-0010

Received July 10, 2007

Density functional theory has been used to study the electronic spin-state properties of low-spin $Fe[HB(pz)_3]_2$, high-spin $Fe[HB(3\text{-}Mepz)_3]_2$, high-spin $Fe[HB(3,5\text{-}Me_2pz)_3]_2$, and high-spin $Fe[HB(3,4,5\text{-}Me_3pz)_3]_2$ complexes that exhibit very different iron(II) electronic spin-sate crossover behaviors with changing temperature and pressure. Excellent agreement is obtained between the experimentally observed Mössbauer-effect quadrupole splittings and isomer shifts of these complexes and those calculated with the B3LYP functional and various different basis sets for both the high-spin and low-spin states of iron(II). The calculations for $Fe[HB(pz)_3]_2$ that use the LANL2DZ, 6-31++G(d,p), and 6-311++G(d,p) basis sets for iron all lead to very similar electric field gradients and thus quadrupole splittings. The initial calculations, which were based upon the known X-ray structures, were followed by structural optimization, an optimization that led to small increases in the Fe−N bond distances. Optimization led to at most trivial changes in the intraligand bond distances and angles. The importance of the 3-methyl−H···H−3-methyl nonbonded intramolecular interligand interactions in controlling the minimum Fe−N bond distances and determining the iron(II) spin state both in $Fe[HB(3\text{-}Mepz)_3]_2$ and in the related methyl-substituted complexes has been identified.

Introduction

The low-spin and high-spin complexes of iron(II) exhibit[1] completely different Mössbauer spectra because of their very different electronic properties; see Figure 1. In the case of low-spin octahedral or pseudooctahedral iron(II) complexes, with a t_{2g}^6 electronic configuration and a $^1A_{1g}$ electronic ground state, the spherical $3d^6$ electron density yields a zero-valence contribution, q_{val}, to the electric field gradient at the iron-57 nucleus; the resulting spectra exhibit a small quadrupole splitting, ΔE_Q, typically of $\pm 0.1-0.4$ mm/s. The small observed quadrupole splitting results from a lattice contribution, q_{lat}, to the electric field gradient, a contribution that is known[2] to result predominately from distortions in the local iron(II)-to-ligand bond distances rather than from intermolecular interactions.

In contrast, for high-spin octahedral or pseudooctahedral iron(II) complexes, with a $t_{2g}^4e_g^{*2}$ electronic configuration and a nominal $^5T_{2g}$ electronic ground state, any nonspherical $3d^6$ electron density resulting from a low-symmetry component to the octahedral crystal field yields a nonzero valence contribution, q_{val}, to the electric field gradient at the iron-57 nucleus; the resulting spectra, depending upon the extent of the distortion, may exhibit quadrupole splittings ranging in magnitude from zero to several millimeters per second. In this case, the observed quadrupole splitting results from the sum of the typically small lattice contribution and a zero to large valence contribution to the electric field gradient. In general, these two contributions are observed[3] to have different signs, and thus the lattice contribution reduces somewhat the magnitude of the valence contribution and thus the observed magnitude of ΔE_Q. This division into two contributions to the quadrupole splitting is very common in the

* To whom correspondence should be addressed. E-mail: glong@mst.edu.
† Department of Chemistry, University of Liège. E-mail: fremacle@ulg.ac.be.
‡ Department of Physics, University of Liège. E-mail: fgrandjean@ulg.ac.be.
§ University of Missouri.

(1) Gütlich, P., Goodwin, H. A., Eds. *Spin Crossover in Transition Metal Compounds I−III*; Springer-Verlag: Berlin, Germany, 2004.
(2) Reger, D. L.; Gardinier, J. R.; Elgin, J. D.; Smith, M. D.; Hautot, D.; Long, G. J.; Grandjean, F. *Inorg. Chem.* **2006**, *45*, 8862–8875.
(3) Ingalls, R. *Phys. Rev.* **1964**, *133A*, 787–795.

10.1021/ic701367b CCC: $40.75
Published on Web 04/18/2008

Mössbauer-effect literature.[4–7] The interpretation of the Mössbauer hyperfine parameters, i.e., the quadrupole splitting and isomer shift, through density functional theory (DFT) calculations renders such a simple division obsolete because the electric charge distribution and the electric field gradient at the iron nucleus are simultaneously calculated, including the electronic charge on the iron ion and all of the remaining constituents of the complex.

The very different shielding of the 3s and 4s electrons of iron(II) by the high-spin $t_{2g}^4e_g^{*2}$ and low-spin t_{2g}^6 electronic configurations yields very different *n*s electronic densities at the iron-57 nucleus. As a result, octahedral high-spin iron(II) complexes typically have 295 K isomer shifts of ca. 1.00−1.15 mm/s, whereas the low-spin complexes have isomer shifts of ca. 0.40−0.50 mm/s; these isomer shifts are given relative to a room temperature α-iron foil. In this context, it should be noted that the higher the isomer shift, the lower are the *n*s electronic densities at the iron-57 nucleus.

As is illustrated in Figure 1, the various iron(II) complexes of tris(pyrazolylborate)[7–13] exhibit very different isomer shifts and quadrupole splittings in their high-spin and low-spin states. The two crystallographically distinct but very similar iron(II) sites in $Fe[HB(pz)_3]_2$ (**1**) have average Fe−N bond distances of 1.975(3) and 1.970(3) Å at room temperature,[14] and both sites remain low-spin from 4.2 to ca. 420 K.[12,13] However, both of the iron(II) sites in **1** undergo a spin-state transition to the high-spin state above ca. 420 K.[13] In contrast, $Fe[HB(3,5\text{-}Me_2pz)_3]_2$ (**2**) has an average room temperature Fe−N bond distance[14] of 2.172(4) Å and is low-spin below and high-spin above ca. 150 K.[11] Presumably, intramolecular interligand H···H nonbonded interactions between the 3-methyl groups on the pyrazolyl moiety in **2**, interactions that are absent in **1**, prevent the close approach of the ligands and maintain the high-spin state above 150 K. For the same reason, the related $Fe[HB(3\text{-}Mepz)_3]_2$ (**3**) complex[15] is also high-spin at room temperature with an average Fe−N bond distance of 2.2011(5) Å. Finally, $Fe[HB(3,4,5\text{-}Me_3pz)_3]_2$ (**4**) remains high-spin upon cooling[12] from 293 to 1.7 K and has an average Fe−N bond distance of 2.190(4) Å at 150 K.[2]

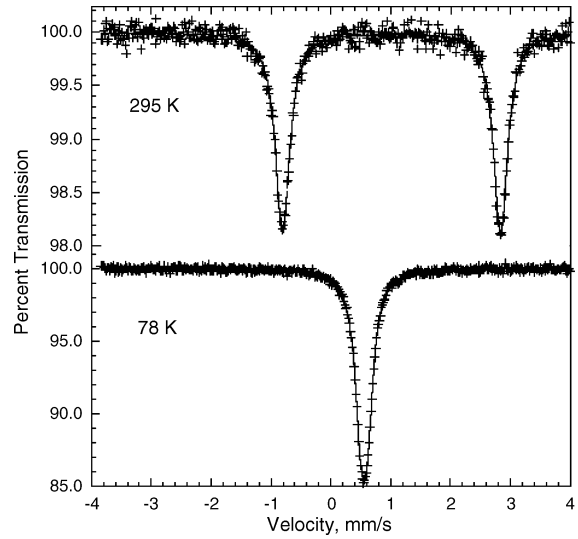

Figure 1. Mössbauer spectra of **2** obtained in the high-spin state at 295 K and in the low-spin state at 78 K.

Because of the very different isomer shifts and quadrupole interactions observed[7–13] in the various iron(II) pyrazolylborate complexes and because of the importance of intramolecular interligand interactions, we have undertaken DFT calculations on these complexes whose X-ray structures are known.[14,15] Although there have been earlier reports[16–18] of the DFT calculations on iron(II) complexes, to the best of our knowledge, the only previous DFT calculations on any complexes related to iron(II) pyrazolylborate are those reported by Paulsen and coworkers,[19–21] who studied the differences in entropy, vibrational energy, and total energy for the reportedly low-spin $\{Fe[HC(R\text{-}pz)_3]_2\}^{2+}$ complexes, where the R substituent is H, 3-Me, 4-Me, 4-Br, or 5-Me. Unfortunately, these authors did not compare their results with the experimental results reported by Reger et al.[22]

It is well-known[1] that the spin-state properties of many iron(II) complexes, including some iron(II) pyrazolylmethane complexes,[23] are very dependent upon the anion present. However, it should be noted that the iron(II) pyrazolylborate complexes under study herein have the advantage of being

(4) DeBenedetti, S.; Lang, G.; Ingalls, R. *Phys. Rev. Lett.* **1961**, *6*, 60–62.
(5) Danon, J. In *Chemical Applications of Mössbauer Spectroscopy*; Goldanskii, V. I., Herber, R. H., Eds.; Academic Press: New York, 1968; pp 159–267.
(6) Gütlich, P. In *Mössbauer Spectroscopy*; Gonser, U., Ed.; Springer-Verlag: Berlin, Germany, 1975; pp 53–96.
(7) Trofimenko, S. *Scorpionates: The Coordination Chemistry of Polypyrazolylborate Ligands*; Imperial College Press: London, 1999.
(8) Jesson, J. P.; Trofimenko, S.; Eaton, D. R. *J. Am. Chem. Soc.* **1967**, *89*, 3158–3164.
(9) Jesson, J. P.; Weiher, J. F.; Trofimenko, S. *J. Chem. Phys.* **1968**, *48*, 2058–2066.
(10) Trofimenko, S. *Chem. Rev.* **1993**, *93*, 943–980.
(11) Long, G. J.; Grandjean, F.; Reger, D. L. In *Spin Crossover in Transition Metal Compounds I*; Gütlich, P., Goodwin, H. A., Eds.; Springer-Verlag: Berlin, Germany, 2004; p 93.
(12) Long, G. J.; Hutchinson, B. B. *Inorg. Chem.* **1987**, *26*, 608–613.
(13) Grandjean, F.; Long, G. J.; Hutchinson, B. B.; Ohlhausen, L.; Neill, P.; Holcomb, J. D. *Inorg. Chem.* **1989**, *28*, 4406–4414.
(14) Oliver, J. D.; Mullica, D. F.; Hutchinson, B. B.; Milligan, W. O. *Inorg. Chem.* **1980**, *19*, 165–169.
(15) Calogero, S.; Gioia Lobbia, G.; Cecchi, P.; Valle, G.; Friedl, J. *Polyhedron* **1994**, *97*, 87–97.
(16) Havlin, R. H.; Godbout, N.; Salzmann, R.; Wojdelski, M.; Arnold, W.; Schultz, C. E.; Oldfield, E. *J. Am. Chem. Soc.* **1998**, *120*, 3144–3151.
(17) Godbout, N.; Havlin, R. H.; Salzmann, R.; Debrunner, P. G.; Oldfield, E. *J. Phys. Chem. A* **1998**, *102*, 2342–2350.
(18) Zhang, Y.; Oldfield, E. *J. Phys. Chem. A* **2003**, *107*, 4147–4150. Zhang, Y.; Mao, J.; Oldfield, E. *J. Am. Chem. Soc.* **2002**, *124*, 7829–7839.
(19) Paulsen, H.; Trautwein, A. X. *J. Phys. Chem. Solids* **2004**, *65*, 793–798.
(20) Paulsen, H.; Trautwein, A. X. In *Spin Crossover in Transition Metal Compounds III*; Gütlich, P., Goodwin, H. A., Eds.; Springer-Verlag: Berlin, Germany, 2004; p 197.
(21) Paulsen, H.; Duelund, L.; Winkler, H.; Toftlund, H.; Trautwein, A. X. *Inorg. Chem.* **2001**, *40*, 2201–2203.
(22) Reger, D. L.; Little, C. A.; Rheingold, A. L.; Lam, M.; Liable-Sands, M.; Rhagitan, B.; Concolino, T.; Mohan, A.; Long, G. J.; Briois, V.; Grandjean, F. *Inorg. Chem.* **2001**, *40*, 1508–1520.
(23) Reger, D. L.; Little, C. A.; Smith, M. D.; Rheingold, A. L.; Lam, K.-C.; Concolino, T. L.; Long, G. J.; Hermann, R. P.; Grandjean, F. *Eur. J. Inorg. Chem.* **2002**, 1190–1197.

molecular complexes, and thus no anions are involved in the calculations.

The goal of this work is, first, to calculate the electric field gradients and isomer shifts in these complexes and to compare the results with the experimental results obtained from Mössbauer spectroscopy. Second, we hope to gain a better understanding of the intramolecular interactions in these complexes, and eventually in related complexes,[24,25] interactions that control the electronic spin state.

Computational Methods

DFT calculations using the *Gaussian03* quantum chemical program[26] have been carried out with the B3LYP functional and the relativistic electron-core double-ζ LANL2DZ pseudopotentials[27] for iron. Earlier reports[16–18,28] have indicated that the B3LYP functional is the most reliable for the study of iron(II) complexes. Further, the computations on complex **1** have been carried out with several different basis sets (see Table S1 in the Supporting Information), including the LANL2DZ, 6-31++G(d,p), and 6-311++G(d,p) Gaussian basis sets for iron and the 6-31++G(d,p) and 6-311++G(d,p) Gaussian basis sets for hydrogen, boron, carbon, and nitrogen. In all tables, the 6-31++G(d,p) and 6-311++G(d,p) Gaussian basis sets used for iron are indicated by full and W, respectively, and no designation corresponds to the LANL2DZ basis set for iron.

For the larger molecules **2**−**4**, the LANL2DZ basis set has been used for iron and the 6-31G(d) basis set has been used for hydrogen, boron, carbon, and nitrogen. In addition, single-point computations for the X-ray structures and the structures optimized at the LANL2DZ/6-31G(d) level have been carried out at the 6-311++G(d,p) level. The small 6-31G(d) basis set includes empty d orbitals on the non-hydrogen atoms, whereas the larger 6-311++G(d,p) basis set also includes diffuse functions on all atoms and empty p orbitals on hydrogen. For the high-spin iron(II) quintet state, unrestricted DFT calculations have been used with a different set of molecular orbitals for the α-spin and β-spin electrons.

A single-point electronic energy computation was used for the single-crystal X-ray structures, followed by a structural optimization. All computations have been constrained to either the singlet or quintet state, states that correspond to the low-spin and high-spin iron(II) states, respectively. The electronic structure calculations were carried out with the *Gaussian03* keywords int = Ultrafine and SCF = tight. For the geometry optimizations, all of the vibrational frequencies were checked and found to be positive. The accuracy associated with the optimized bond lengths will depend upon the use of either a pseudopotential or a full-electron basis set. In general, the accuracy of the bond lengths[29] obtained at the DFT level with an all-electron basis set is $\pm 0.01-0.005$ Å; both Neese and co-workers[30,31] and Schaefer and co-workers[32,33] have observed error limits of ± 0.02 Å for some iron complexes and organometallic compounds. More recently, Schwerdtfeger et al.[28] reported iron−ligand bond lengths in $Fe(CO)_5$, $FeCl_2$, and $FeBr_2$ that are longer in the optimized B3LYP calculations by 0.014, 0.019, and 0.024 Å, respectively, than the experimental bond lengths. Optimized bond lengths obtained with different functionals are also observed to be longer than the experimental bond lengths. These systematic bond length increases upon optimization, increases that are independent of the functional used, remain within the accuracy given above of the calculations reported herein.

The natural orbital populations have been calculated by using the method of Carpenter and Weinhold,[34] and the tensor representation of the electric field gradients has been calculated by the method of Barone.[35] A pseudopotential cannot be used to calculate $\rho(0)$, the electron density at the iron-57 nucleus, the density that determines the Mössbauer-effect isomer shift. Thus, in order to calculate these values,[36] single-point computations based both on the X-ray structure and on the optimized geometry obtained with the LANL2DZ pseudopotentials for **1**−**3** have also been carried out with the 6-311++G(d,p) basis set by using the *Gaussian03* cubegen full-density option to calculate the full electron-core density, $\rho(0)$, at the iron-57 nucleus.

Scalar relativistic effects are expected[37] to be large especially for the 1s and 2s core electrons of the iron-57 nucleus, and therefore relativistic effects affect significantly the absolute value of $\rho(0)$, which is underestimated when using a nonrelativistic Hamiltonian, such as the Kohn–Sham Hamiltonian used herein. Early work[38] has indicated that the relativistic correction is element-dependent but electronic-configuration-independent, and these authors proposed multiplication of the nonrelativistic $\rho(0)$, obtained at the Hartree–Fock level, by an element-dependent scaling factor, $S(Z)$, which they estimated to be 1.3−1.4 for iron. Unfortunately, the exact treatment of relativistic effects for large molecules remains, even today, computationally out of reach, and several approximate quasi-relativistic methods have been developed.[37] In addition to the problems resulting from the neglect of relativistic effects, nonrelativistic calculations present additional problems, such as those that arise from the use of Gaussian basis sets that poorly reproduce the electron density cusps at the nuclei and the variation of the absolute value of $\rho(0)$ with the functional used in the nonrelativistic Hamiltonian. However, nonrelativistic treatments, in general, give relative $\rho(0)$ values that are in good agreement with experimental values, as is the case herein. As a consequence,

(24) Reger, D. L.; Gardinier, J. R.; Bakbak, S.; Gemmill, W.; Smith, M. D.; Rebbouh, L.; Grandjean, F.; Shahin, A. M.; Long, G. J. *J. Am. Chem. Soc.* **2005**, *127*, 2303–2316.

(25) Reger, D. L.; Gardinier, J. R.; Smith, M. D.; Shahin, A. M.; Long, G. J.; Rebbouh, L.; Grandjean, F. *Inorg. Chem.* **2005**, *44*, 1852–1866.

(26) Frisch, M. J.; Trucks, G. W.; Schlegel, H. B.; Scuseria, G. E.; Robb, M. A.; Cheeseman, J. R.; Zakrzewski, V. G.; Montgomery, J. A.; Stratmann, R. E.; Burant, J. C.; Dapprich, S.; Millan, J. M.; Daniels, A. D.; Kudin, K. N.; Strain, M. C.; Farkas, O.; Tomasi, J.; Barone, V.; Cossi, M.; Cammi, R.; Mennucci, B.; Pomelli, C.; Adamo, C.; Clifford, S.; Ochterski, J.; Peterson, G. A.; Ayala, P. Y.; Cui, Q.; Morokuma, K.; Malick, D. K.; Rabuck, A. D.; Raghavachari, K.; Foresman, J. B.; Cioslowski, J.; Ortiz, J. V.; Stefanov, B. B.; Liu, G.; Liashenko, A.; Piskorz, P.; Komaromi, I.; Gomperts, R.; Martin, R. L.; Fox, D. J.; Keith, T.; Al-Laham, M. A.; Peng, C. Y.; Nanayakkara, A.; Gonzalez, C.; Challacombe, M.; Gill, P. M. W.; Johnson, B. G.; Chen, W.; Wong, M. W.; Andres, J. L.; Head-Gordon, M.; Replogle, E. S.; Pople, J. A. *Gaussian03*, revision B.1; Gaussian Inc.: , Pittsburgh, PA, 2003.

(27) Hay, P. J.; Wadt, W. R. *J. Chem. Phys.* **1985**, *82*, 270–283. **1985**, *82*, 299–310.

(28) Schwerdtfeger, P.; Söhnel, T.; Pempointner, M.; Laerdahl, J. K.; Wagner, F. E. *J. Chem. Phys.* **2001**, *115*, 5913–5924.

(29) Engel, T. *Quantum Chemistry and Spectroscopy*; Pearson-Benjamin Cummings: San Francisco, CA, 2006.

(30) Neese, F. *J. Biol. Inorg. Chem.* **2006**, *11*, 702–711.

(31) Berry, J. F.; Bill, E.; Bothe, E.; George, S. D.; Mienert, B.; Neese, F.; Wieghardt, K. *Science* **2006**, *312*, 1937–1941.

(32) Wang, H.; Xie, Y.; King, R. B.; Schaefer, H. F., III *J. Am. Chem. Soc.* **2005**, *127*, 11646–11651.

(33) Wang, H.; Xie, Y.; King, R. B.; Schaefer, H. F., III *J. Am. Chem. Soc.* **2006**, *128*, 11376–11384.

(34) Carpenter, J. E.; Weinhold, F. *THEOCHEM* **1988**, *46*, 41–62.

(35) Barone, V. *Chem. Phys. Lett.* **1996**, *262*, 201–206.

(36) Neese, F. *Inorg. Chim. Acta* **2002**, *337*, 181–192.

(37) Neese, F.; Wolf, A.; Fleig, T.; Reiher, M.; Hesse, B. A. *J. Chem. Phys.* **2005**, *122*, 204107. (10 pages) and references cited therein.

(38) Freemann, A. J.; Ellis, D. E. In *Mössbauer Isomer Shifts*; Shenoy, G. K., Wagner, F. E., Eds.; North-Holland: Amsterdam, The Netherlands, 1978; pp 111–201.

Table 1. Calculated Natural Charges and Electronic Configurations

complex	structure	multiplicity	charge	electronic configuration
1	Fe1, X-ray structure[a]	singlet	0.58	$[Ar]4s^{0.28}3d^{7.12}5s^{0.02}4d^{0.02}$
	Fe2, X-ray structure[a]	singlet	0.58	$[Ar]4s^{0.28}3d^{7.13}5s^{0.02}4d^{0.02}$
	Fe1, X-ray structure,[a] full	singlet	0.62	$[Ar]4s^{0.30}3d^{6.98}6s^{0.01}4d^{0.08}4p^{0.02}7p^{0.01}$
	Fe1, X-ray structure,[a] W	singlet	0.63	$[Ar]4s^{0.28}3d^{7.01}4d^{0.07}4p^{0.01}$
	Fe1, optimized	singlet	0.68	$[Ar]4s^{0.27}3d^{7.03}5s^{0.02}4d^{0.01}$
	Fe2, optimized	singlet	0.68	$[Ar]4s^{0.27}3d^{7.03}5s^{0.02}4d^{0.01}$
	Fe1, optimized	quintet	1.45	$[Ar]4s^{0.28}3d^{6.26}5s^{0.00}4d^{0.01}4p^{0.01}$
	Fe1, optimized, full	singlet	0.65	$[Ar]4s^{0.30}3d^{6.95}6s^{0.01}4d^{0.07}4p^{0.02}$
	Fe1, optimized, W	quintet	1.39	$[Ar]4s^{0.23}3d^{6.27}4d^{0.05}$
3	X-ray structure[b]	quintet	1.45	$[Ar]4s^{0.25}3d^{6.26}5s^{0.01}4d^{0.01}$
	X-ray, 3-Me- stag-eclip[b]	quintet	1.45	$[Ar]4s^{0.25}3d^{6.28}5s^{0.01}4d^{0.01}$
	X-ray, 3-Me- staggered[b]	quintet	1.45	$[Ar]4s^{0.25}3d^{6.27}5s^{0.01}4d^{0.01}$
	optimized, 146°	quintet	1.47	$[Ar]4s^{0.25}3d^{6.26}5s^{0.01}4d^{0.01}$
	optimized, 146°	singlet	0.77	$[Ar]4s^{0.23}3d^{6.97}5s^{0.00}4d^{0.02}5p^{0.02}$
2	X-ray structure[a]	quintet	0.96	$[Ar]4s^{0.23}3d^{6.79}5s^{0.01}4d^{0.01}$
	optimized, 146°	quintet	1.43	$[Ar]4s^{0.25}3d^{6.30}5s^{0.01}4d^{0.01}$
	optimized, 146°	singlet	0.96	$[Ar]4s^{0.23}3d^{6.79}4d^{0.01}5p^{0.01}$
4	X-ray structure[c]	quintet	1.45	$[Ar]4s^{0.25}3d^{6.28}4p^{0.01}4d^{0.01}$
	X-ray structure[c]	singlet	1.02	$[Ar]4s^{0.23}3d^{6.73}4d^{0.01}5p^{0.01}$
	optimized, 146°	quintet	1.44	$[Ar]4s^{0.25}3d^{6.29}4p^{0.01}4d^{0.01}$
5	X-ray structure[d]	singlet	–0.115	$[Ar]4s^{0.01}3d^{7.62}4p^{0.03}5s^{0.45}4d^{0.03}$
	optimized	singlet	–0.042	$[Ar]4s^{0.01}3d^{7.53}4p^{0.03}5s^{0.45}4d^{0.03}$

[a] Structure obtained from ref 14. [b] Structure obtained from ref 15. [c] 150 K structure obtained from ref 2. [d] Structure obtained from ref 39.

the $\rho(0)$ values reported herein correspond to the "bare" nonrelativistic values obtained with the B3LYP functional and the 6-311++G(d,p) basis set with no further scaling.

In order to determine the calculated isomer shifts relative to one of the iron-57 Mössbauer-effect reference standards, the same single-point and optimized geometry computations have been carried out on the $[Fe(CN)_5NO]^{2-}$ anion (**5**) of sodium nitroprusside (SNP), the iron-57 Mössbauer-effect primary reference standard whose X-ray structure is known.[39]

Results and Discussion

The single-crystal X-ray structures[2,14,15,39] of the four iron(II) complexes under study, namely, low-spin **1**, high-spin **3**, high-spin **2**, and high-spin **4**, as well as of **5**, have been used as the input structures for all of the calculations reported herein. In the initial single-point calculations, the structures were constrained to those of the reported room temperature X-ray structures for **1**−**3** and **5** and the 150 K structure for **4**. Further, for each computation, the spin multiplicity has been constrained to either the singlet or quintet state.

The 0 K calculated X-ray structure based total molecular energies, X-ray structural features, and resulting charges and calculated electronic configurations are listed as the X-ray structure results in Tables S2 and S3 in the Supporting Information and 1, respectively. These tables also contain the results for the subsequent optimized structure, an optimization process in which the total molecular energy was minimized through structural modifications of the X-ray structure with the specified spin multiplicity. The results will now be discussed, in turn, for the individual complexes. In order to make the results easier to assimilate, each of the tables has been presented, as far as possible, with the same format as that used in Table 1.

The differences between the optimized structure and the results obtained for the X-ray structure (see Table S3 in the Supporting Information) may be considered to represent the difference between the ideal minimum energy 0 K gas-phase molecular structure and the molecular structure at a finite temperature in the presence of solid-state lattice interactions. For each molecule, upon optimization, the overall symmetry of the molecule has increased and the volume of the molecular structure has expanded by as much as ∼10%, a dramatic increase that is accompanied by substantially longer Fe−N bonds; a similar Fe−N bond length increase has been reported by Zein et al.[40]

The increases in the Fe−N bond distances are approximately twice as large as the computational accuracy for the four iron(II) complexes, whereas no significant increase is observed for the optimized geometry of **5**.

The molecular expansion found upon structural optimization reduces the total energy by as much as ∼10 eV, a surprisingly large reduction. It is difficult to determine how much influence the basis set has upon the total energy, but the decreases in energy upon structural optimization obtained herein are internally consistent for the different basis sets used. Unfortunately, the reduction in the total energy upon structural optimization was not reported in the earlier work,[16–18,28,30,31,36,37,41] and no comparison is thus possible. Further, it should be noted that all of the calculated vibrational frequencies of the complexes studied herein have been found, as must be the case, to be positive in the optimized structures; a similar finding was not mentioned in the earlier work.[16–18,28,30,31,36,37,41]

At this point, it should be noted that no spin-state crossover is observed for the energy of any of the complexes studied herein, presumably because the calculations correspond to the gaseous state and thus cannot reflect any extended lattice cooperative interactions, interactions that are usually associated with the spin-state crossover phenomenon. However,

(39) Manoharan, P. T.; Hamilton, W. C. *Inorg. Chem.* **1963**, *2*, 1043–1047.
(40) Zein, S.; Matouzenko, G. S.; Borshch, S. A. *Chem. Phys. Lett.* **2004**, *397*, 475–478.
(41) Neese, F. *Curr. Opin. Chem. Biol.* **2003**, *7*, 125–135.

the differences in the energy, $E_{quintet} - E_{singlet}$, of the high-spin quintet state and the low-spin singlet state for the optimized structures do reveal a weak correlation with the spin-state crossover temperatures observed in the complexes under study. These energy difference (see Table S2 in the Supporting Information) are +1(8) kJ/mol for **1**, –30(8) kJ/mol for **3**, –25(8) kJ/mol for **2**, and –79(8) kJ/mol for **4**. The corresponding spin-state crossover temperatures[2] are 343−390 K for **1**, 85 K for **3**, and 190 K for **2**; **4** remains high-spin above 1.7 K but is gradually converted to the low-spin state at applied pressures above ca. 20 kbar.[12]

Complex 1. The single-crystal X-ray structure[14] of low-spin **1** has two structurally very similar, but crystallographically distinct, Fe1 and Fe2 sites. This added structural complexity makes a comparison of the results of the DFT calculations possible on what are two essentially very similar molecules, molecules that exhibit identical Mössbauer spectral isomer shifts and quadrupole splittings. Thus, single-point and structural optimization calculations have been carried out for both Fe1 and Fe2 crystallographic sites in **1**. As may be observed in Table S2 in the Supporting Information, the calculated total molecular energies of the Fe1 and Fe2 molecules are, as expected, the same within the computational accuracy[42,43] of ca. ±0.0030 au, ±0.08 eV, or ±8 kJ/mol. Even more important, Tables 1 and S2 and S3 in the Supporting Information indicate that the optimized molecular structures resulting from the Fe1 and Fe2 input X-ray structures are virtually identical in total energy, structure, charge, and electronic configuration. As will be discussed below, this comparison has also been useful in establishing approximate error limits for the electric field gradient calculations.

The total molecular energy of **1** is lowered by ca. 840(8) kJ/mol in going from the X-ray structure to the optimized structure; see Table S2 in the Supporting Information for complete details. By far, the most significant difference between the X-ray and optimized structures of **1** occurs in the expansion of the average Fe−N bond distance from 1.970 or 1.975 Å to 2.021 Å, an expansion of 2.5%, which is similar to the expansion calculated by Zein et al.[40] At the same time, the Fe–B intraligand nonbonded distance expands on average from 3.080 to 3.112 Å, an expansion of 1.1%, but, perhaps surprisingly, the remaining structural features of the ligands are relatively unchanged. The concentration of the expansion at the Fe−N bonds may result because the most "empty" space in the molecule is found in the vicinity of the iron(II) ion. Further, the intramolecular interligand H···H nonbonded distance remains approximately the same at 3.325 Å, where the hydrogens are on the 3 position of the pyrazolyl ring. It is this "close" H···H approach that permits the rather short ca. 1.97 Å Fe−N bond distance, a close approach that generates a larger crystal field at the iron(II) ion and thus the low-spin electronic state observed for **1** below ca. 430 K. Substitution of a methyl at this position forces the resulting complex to have much longer Fe−N bond distances and thus to be high-spin.

One would nominally expect an iron charge of 2+ and an $[Ar]4s^0 3d^6$ electronic configuration for **1**, as well as the remaining complexes under study. Thus, it is rather surprising that DFT calculations based on a natural atomic orbital analysis[34] yield charges of only 0.58+ and 0.68+ for the iron(II) in the X-ray structure and the optimized structure of **1**, respectively. The corresponding electronic configurations are $[Ar]4s^{0.28}3d^{7.12}5s^{0.02}4d^{0.02}$ and $[Ar]4s^{0.27}3d^{7.03}5s^{0.02}4d^{0.01}$. The difficulty in assigning atomic charges from an electronic structure computation is well-known[42] and results from the problem of formally dividing the bonding electron density between different specific atoms or ions in a molecule. The observed electronic configurations do, however, seem rather reasonable, especially in view of the electric field gradients generated at the iron nucleus, gradients that agree quite well with the Mössbauer-effect quadrupole splittings discussed below.

Three different basis sets have been used for the iron(II) in **1**, namely, the relativistic energy consistent Hay−Wadt pseudopotentials[27] with a double-ζ LANL2DZ basis set and the two full-electron Gaussian basis sets, the double-ζ, 6-31+G(d) basis set and the triple-ζ Wachters−Hay 6-311+G(d) basis set,[44,45] provided with *Gaussian03*. These results are summarized near the top of Tables 1 and S2 and S3 in the Supporting Information. Rather nicely, for computations using different basis sets, the iron(II) charges and electronic configurations are quite similar.

Finally, the structure of **1** has been optimized under the assumption that it has a quintet state. The most interesting result in the calculation for this pseudoelectronic spin state is the resulting average Fe−N bond distance of 2.211 Å, a distance that is only slightly larger than those typically observed[1,14,15] in high-spin iron(II) complexes; see Table S3 in the Supporting Information for full details. In contrast, and unexpectedly, as is revealed by the results given in Table S2 in the Supporting Information, the energy difference between the two spin states, $E_{quintet} - E_{singlet}$, is +1(8) kJ/mol at 0 K, when no zero-point vibrational energy correction is applied. After correction, the quintet state is barely significantly more stable than the singlet state at $E_{quintet} - E_{singlet} = -8(8)$ kJ/mol. Apparently, as noted earlier,[16–18] DFT calculations on an isolated molecule do not reveal the energy differences expected of the two spin states, but it should be noted that **1** is known to undergo a spin-state crossover to the high-spin iron(II) state at 420 K.[13]

Complex 3. Preliminary studies on **2** revealed serious difficulties in convergence of the optimized structure because of small rotations of the 5-methyl hydrogen positions. As a consequence, it was decided to first study **3**, in which this problem could be avoided. This molecule also has two chemically similar, but crystallographically distinct, iron(II) sites,[15] and only the Fe2 site has been studied herein.

In studying the crystallographically determined positions of the hydrogens on the 3-methyl groups in **3**, it was apparent

(42) Cramer, C. J. *Essentials of Computational Chemistry*; Wiley: Chichester, U.K., 2003.
(43) Ratner, M. A.; Schatz, G. C. *Introduction to Quantum Mechanics in Chemistry*; Prentice-Hall: New York, 2001.
(44) Wachters, A. J. H. *J. Chem. Phys.* **1970**, *52*, 1033–1036.
(45) Hay, P. J. *J. Chem. Phys.* **1977**, *66*, 4377–4384.

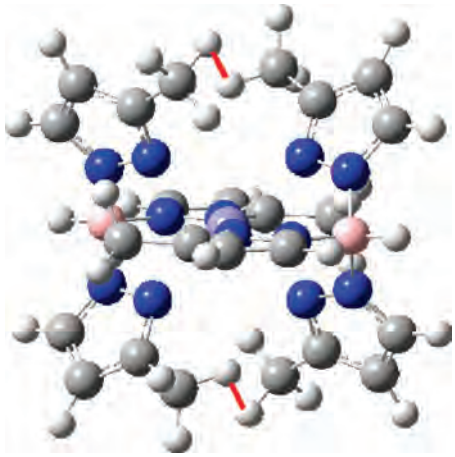

Figure 2. Molecular structure of **3** in an orientation showing the two $HB(3,5\text{-}Me_2pz)_3$ ligands on the left and right, respectively, with iron(II) in light blue, nitrogen in dark blue, boron in pink, and carbon in gray. The red lines show two of the three 3-methyl–3-methyl H···H nonbonded interactions between the two different $HB(3,5\text{-}Me_2pz)_3$ ligands.

that these positions were poorly determined in the reported[15] X-ray structure. So, the "riding-hydrogen" feature of *GaussView*[46] was used to initially place the three hydrogens on the carbon of the 3-methyl groups. Next, two rotational conformations of this 3-methyl group were used for optimization of the structure. In the first, the hydrogens were in alternatively staggered and eclipsed orientations, whereas in the second, they were all in the staggered orientation. In this context, the staggered and eclipsed conformations are defined with respect to the 3-methylpyrazole intraligand H–C···C–H dihedral angle, where the first H and C are on the 3-methyl moiety and the second C and H correspond to the carbon and hydrogen at the 4 position of the pyrazolyl ring. If this dihedral angle is 180°, the conformation is staggered, and if it is 0°, the conformation is eclipsed. The total energies and electronic properties of these two constrained conformations are given in Tables 1 and S2 in the Supporting Information. One would expect that the staggered conformation would give the lowest energy, as is indeed the case; see Table S2 in the Supporting Information. However, in reality, the most important factor determining the minimum energy is the 3-methyl–3-methyl H···H nonbonded intramolecular interligand interaction. Two out of three of these interactions are shown by the two red lines connecting the 3-methyl–3-methyl H···H nonbonded atoms in the two different ligands in **3**; see Figure 2. A subsequent full structural optimization indicated that a H–C···C–H dihedral angle of 146° corresponded to the minimum in the total molecular energy; see Table S2 in the Supporting Information.

The results for the constrained X-ray structure and the optimized 146° structure in the quintet and singlet states of **3** are given in Tables 1 and S2 and S3 in the Supporting Information and reveal a decrease in the energy of the optimized structure by 107(10) kJ/mol, a decrease that is associated with an increase in the average Fe−N bond distance of 0.031 Å or 1.4% from 2.208 to 2.239 Å. The charge of the iron in the optimized quintet structure is 1.47, a value that is low but perhaps reasonable for an iron(II) ion considering the computational difficulties in determining this charge. The optimized $[Ar]4s^{0.25}3d^{6.26}5s^{0.01}4d^{0.01}$ electronic configuration is very close to what would be expected in a high-spin iron(II) complex. Except for the increase in the Fe−N average bond distance, as was the case for **1**discussed above, there seems to be very little structural change in the ligand upon optimization of the X-ray structure. However, in the optimized structure, there is a distinct increase of 0.219 Å or 8.3% from 2.642 to 2.861 Å in the intramolecular interligand 3-methyl–3-methyl H···H nonbonded distance. It is this nonbonded 2.642 Å interaction distance that presumably maintains the long Fe−N bond distance and thus the high-spin state observed[15] in **3** at 295 K.

For **3**, the energy difference between the two spin states, $E_{quintet} - E_{singlet}$ is –30(8) kJ/mol at 0 K, when no zero-point vibrational energy correction is applied. After zero-point vibrational energy correction, the quintet state is still more stable than the singlet state at $E_{quintet} - E_{singlet} = -39(8)$ kJ/mol. A similar energy difference has been observed by Zein et al.[40] for another spin-crossover compound.

Complexes 2 and 4. The study of **2** began with the X-ray structure reported earlier;[14] in the solid state, this complex has only one crystallographic iron site. Initial attempts to determine the optimized structure failed, and thus the conformation of the 3-methyl group was initially constrained to that of the 146° H–C···C–H conformation found for **3** and the conformation of the 5-methyl group was initially constrained to that reported in the X-ray structure. These constraints were subsequently released to yield the optimized results presented in Tables 1 and S2 and S3 in the Supporting Information. The initial H–C···C–H dihedral angle remained unchanged at 146° in the optimized structure.

The results for the constrained X-ray structure and the optimized structure of **2** again reveal a decrease in the energy of the complex but, in this case, a much larger decrease of 1345(10) kJ/mol, a decrease that is associated with a relatively large increase in the average Fe−N bond distance of 0.062 Å or 2.7% from 2.172 to 2.234 Å.

The calculated charge of the quintet state iron increases from 0.96 in the X-ray structure to 1.42 in the optimized structure, a value that is low but essentially identical with that found for **3**. The optimized $[Ar]4s^{0.25}3d^{6.30}5s^{0.01}4d^{0.01}$ electronic configuration is also essentially the same as that observed for the optimized structure **3**.

The various results obtained for **4** are, in general, very similar to those obtained for **3** and **2**. The energy of **4** is lower than those for the other complexes because of the added bond present in the third methyl substituent; as for the other complexes, the optimized quintet state has the lowest energy. It is worth noting that **4** has the longest Fe−N bond distance of these complexes but also exhibits the smallest, perhaps insignificant, bond length expansion upon optimization.

Electric Field Gradients. DFT calculations may be used to determine the electrostatic potential at each atom in a compound, and the second derivatives of this potential with respect to distance yield the electric field gradient at

(46) Frisch, A.; Dennington, R. D.; Nielsen, A. B.; Holder, A. J. *GaussView Reference*; Gaussian, Inc.: Carnegie, PA, 2003.

Table 2. Calculated and Observed Iron(II) Electric Field Gradients and Quadrupole Splittings

			calculated			observed	
complex	structure	multiplicity	V_{zz},[a,b] au	$eQV_{zz}/2$,[a,c] mm/s	η	ΔE_Q, mm/s	η
1	Fe1, X-ray structure	singlet	–0.126(2)	0.204(4)	0.17	+0.20(1)[d]	~0.1
	Fe2, X-ray structure	singlet	–0.124(2)	0.201(4)	0.26	+0.20(1)[d]	~0.1
	Fe1, X-ray structure, full	singlet	–0.053(2)	0.086(4)	0.17	+0.20(1)[d]	~0.1
	Fe1, X-ray structure, W	singlet	–0.119(2)	0.192(4)	0.30	+0.20(1)[d]	~0.1
	Fe1, optimized	singlet	–0.133(2)	0.215(4)	0.00	+0.20(1)[d]	~0.1
	Fe2, optimized	singlet	–0.131(2)	0.212(4)	0.00	+0.20(1)[d]	~0.1
	Fe1, optimized	quintet	+2.207(2)	–3.568(4)	0.01	–3.44(2)[e]	~0.1
	Fe1, optimized, full	singlet	–0.032(2)	0.052(4)	0.02	+0.20(1)[d]	~0.1
	Fe1, optimized, W	quintet	+2.299(2)	–3.717(4)	0.02	–3.44(2)[e]	~0.1
3	X-ray structure	quintet	+2.140(2)	–3.460(4)	0.08	±3.81(1)[f]	
	X-ray, 3-Me-stag-eclip	quintet	+2.131(2)	–3.446(4)	0.14	±3.81(1)[f]	
	X-ray, 3-Me-staggered	quintet	+2.127(2)	–3.439(4)	0.18	±3.81(1)[f]	
	optimized, 146°	quintet	+2.180(2)	–3.525(4)	0.00	±3.81(1)[f]	
	optimized, 146°	singlet	–0.035(2)	0.056(4)	0.01	±0.20(1)[f]	
2	X-ray structure	quintet	+2.109(2)	–3.410(4)	0.17	±3.67(1)[d]	~0.2
	optimized, 146°	quintet	+2.174(2)	–3.515(4)	0.00	±3.67(1)[d]	~0.2
	optimized, 146°	singlet	–0.142(2)	0.230(4)	0.36	±0.12(1)[d]	
4	X-ray structure	quintet	+2.168(2)	–3.506(4)	0.23	–3.80(1)[d]	~0.1
	X-ray structure	singlet	–0.204(2)	0.330(4)	0.31		
	optimized, 146°	quintet	+2.182(2)	–3.528(4)	0.01	–3.80(1)[d]	~0.1
5	X-ray structure	singlet	–1.252(2)	2.025(4)	0.01	1.703(1)[g]	0.0
	optimized	singlet	–1.181(2)	1.910(4)	0.00	1.703(1)[g]	0.0

[a] 1 au is 9.717×10^{21} V/m^2 and corresponds to a $(eQV_{zz})/2$ value of 1.617(100) mm/s if the nuclear quadrupole moment is $0.16(1) \times 10^{-28}$ m^2. [b] In all cases, V_{zz} is coincident with the approximately 3-fold molecular axis. [c] The relative error from the calculation is given. The error including the error in the nuclear quadrupole moment would be ±0.20 mm/s. [d] Values obtained from ref 12. [e] Value obtained for the high-spin state at 430 K from ref 13. [f] Value obtained from ref 2. [g] Value obtained from ref 51.

the atom; the corresponding eigenvectors provide the orientation of the principal axis of this gradient with respect to a molecular axis, such as the pseudo-3-fold symmetry axis present in the compounds under study herein. The principal component of the electric field gradient, V_{zz}, may also be determined experimentally by Mössbauer spectroscopy from the quadrupole splitting, ΔE_Q, at the iron-57 nucleus, where

$$\Delta E_Q = \frac{1}{2} eQV_{ZZ}\sqrt{1+\frac{\eta^2}{3}} \qquad (1)$$

and e is the electron charge, Q is the nuclear quadrupole moment of the iron-57 nuclear excited state, and η is the electric field gradient asymmetry parameter. Thus, a comparison of calculated and experimentally observed electric field gradients provides an excellent test of the validity of the DFT calculations for iron complexes.

From a comparison of the V_{zz} values calculated for the two singlet optimized structures of the Fe1 and Fe2 sites in **1**, the accuracy of the calculated V_{zz} values is estimated to be ca. ±0.002 au and it may be as good as ±0.001 au. Then, the corresponding accuracy of the quadrupole splittings, ΔE_Q, would be ±0.004 mm/s or better; see Table 2. However, the calculated value of ΔE_Q also depends on the value of the nuclear quadrupole moment, Q, used to obtain ΔE_Q from the calculated V_{zz} values. Unfortunately, the value of Q is not well determined, and values ranging from –0.19 to $+0.44 \times 10^{-28}$ m^2 have been reported.[16,28] Currently, the best experimental value[16–18,47] for Q seems to be $0.16(1) \times 10^{-28}$ m^2, the value that has been used in Table 2. The error of $\pm 0.01 \times 10^{-28}$ m^2 in Q corresponds to an error of ±0.2 mm/s in the calculated values of ΔE_Q, an error that is, of course, constant for all values. Thus, in Table 2, we report the relative error in ΔE_Q obtained from the calculation of V_{zz}.

The calculated values of the principal component of the electric field gradient, V_{zz}, in the iron(II) complexes under study are given in Table 2 along with the corresponding calculated quadrupole splittings, ΔE_Q, and asymmetry parameters, η. This table also gives the experimental quadrupole splittings, ΔE_Q, that have been reported[2,12,13] for these complexes, with their signs when known. It should be noted that ΔE_Q depends upon both V_{zz} and η, but the η dependence is very weak; the largest calculated η value found in Table 2 will increase the corresponding ΔE_Q by at most 1%. In all cases, there is either excellent or very good agreement between the calculated and observed quadrupole splittings that agree within better than 10%. Such a level of agreement is similar to that reported earlier[18] and is better than the 20% obtained in another study.[48] When the sign is experimentally known, it is in agreement with the calculated sign. Of particular significance is the difference in magnitude of the calculated V_{zz} and ΔE_Q values in the low-spin and high-spin states. In all cases, as expected and observed experimentally, their calculated magnitudes for the high-spin state are much larger than those for the low-spin state. Further, it should be noted that the calculated high-spin values are positive whereas the low-spin values are negative. This is in agree-

(47) Dufek, P.; Blaha, P.; Schwarz, K. *Phys. Rev. Lett.* **1995**, *75*, 3545–3548.

(48) Wolny, J. A.; Paulsen, H.; Winkler, H.; Trautwein, A. X.; Tuchagues, J. P. *Hyperfine Interact.* **2005**, *166*, 495–498.

Table 3. Calculated Electron Densities at the Iron-57 Nucleus[a] and the Observed Isomer Shifts

complex	structure	multiplicity	$\rho(0)$, au^{-3}	T(obsd), K	δ (obsd),[b] mm/s	δ (295 K), mm/s
1	Fe1, X-ray structure	singlet	11 616.008	295	0.67[c]	0.67
	Fe2, X-ray structure	singlet	11 615.694	295	0.67[c]	0.67
	Fe1, optimized	quintet	11 614.406	430	1.20[c]	1.29
3	X-ray structure	quintet	11 614.410	295	1.27[d]	1.27
	optimized, 146°	quintet	11 614.328	295	1.27[d]	1.27
	optimized, 146°	singlet	11 615.420	85	0.83[d]	0.68
2	optimized, 146°	quintet	11 614.343	295	1.29[c]	1.29
	optimized, 146°	singlet	11 615.451	78	0.75[c]	0.60
5	X-ray structure	singlet	11 618.090	295	0.00	0.00
	optimized	singlet	11 617.834	295	0.00	0.00

[a] All of the $\rho(0)$ values were obtained by using the 6-311++G(d,p) basis set for all of the atoms including iron. [b] The isomer shifts are given relative to SNP, which has an isomer shift of –0.2649(8) mm/s relative to α-iron. [c] Value obtained from ref 12. [d] Value obtained from ref 2.

ment with several experimental studies[11–13,24] that indicate that the signs of V_{zz} and ΔE_Q are different for the high-spin and low-spin states.

There have been a few studies[19,21,48–50] of compounds related to those under study herein. The most useful and detailed study[50] dealt with several dicationic iron(II) complexes with several analogous pyrazolyl methane derivatives that are structurally similar to the molecular complexes studied herein. These authors, who used the B3LYP functional with the 6-311G basis set, calculated quadrupole splittings between 0.01 and 0.12 mm/s for the low-spin complexes and between 3.34 and 3.81 mm/s for the high-spin complexes. In general, their calculated values are similar to, but somewhat larger in magnitude than, the values found in Table 2. It is difficult to make more detailed comparisons because the calculations have used different computational methods for structurally related yet different compounds.

The X-ray structures of all of the complexes under study herein indicate that they have a pseudo-3-fold symmetry axis coincident with the B···Fe···B axis. For all complexes, as expected, the eigenvectors of the diagonalized electric field gradient tensors indicate that the orientation of the calculated V_{zz} is coincident with this direction to within ca. 15°. The resulting asymmetry parameters, η, are small and in rather good agreement with the experimental values of η; see Table 2. Upon structural optimization, the structural symmetry of these complexes increases to D_{3d}, and, of course, the orientation of V_{zz} is coincident with the 3-fold symmetry axis and η is zero.

Electron Probability Density at Iron(II). The Mössbauer-effect isomer shift provides a measure of the s electron density at the iron-57 nucleus relative to that found either in α-iron or in $Na_2[Fe(CN)_5NO]\cdot 2H_2O$, the two standard reference materials for the iron-57 Mössbauer-effect isomer shift.[51] It should be noted that the higher isomer shifts correspond to lower *n*s electron probability densities at the iron-57 nucleus. This s electron probability density is influenced predominately by the *n*s-orbital electronic populations and, to a lesser extent, by the shielding of this *n*s electron density by the intervening 3d electrons. Because of their very different iron(II) electronic configurations, the high-spin and low-spin complexes under study herein have very different isomer shifts.

In general, at 295 K the isomer shifts, relative to α-iron, of the high-spin iron(II) complexes are ca. 1.0 mm/s, whereas those of the low-spin complexes are ca. 0.4 mm/s. Relative to SNP, the U.S. National Bureau of Standards, now NIST, the primary reference standard for iron-57 Mössbauer-effect isomer shifts, the analogous high-spin isomer shifts are ca. 1.25 mm/s, whereas those of the low-spin complexes are ca. 0.65 mm/s; the increase occurs because SNP has an isomer shift[51] of –0.2649(8) mm/s relative to that of α-iron.

The electron probability density, $\rho(0)$, at the iron-57 nucleus has been calculated from the derived wave functions obtained for complexes **1**−**3** under study herein; a summary of the results is given in Table 3. As mentioned in the Computational Methods section, a pseudopotential cannot be used to calculate $\rho(0)$ and, as a consequence, the $\rho(0)$ values reported in this table have been calculated by using the 6-311++G(d,p) basis set for all of the electrons of the iron(II) ion; in the case of **2** and **3**, the structure has been fixed to the optimized 146° structure. Because the calculations involved all of the electrons, they could not be performed for complex **4** because of the very large number of methyl groups and, hence, electrons.

Unfortunately, it is not possible to use the same computational method used herein for complexes **1**–**4** to calculate $\rho(0)$ at the iron nucleus in α-iron, an extended array solid. To overcome this limitation, we have referred all of the isomer shifts to the alternative reference standard, SNP, $Na_2[Fe(CN)_5NO]\cdot 2H_2O$, for which the analogous calculation of $\rho(0)$ at the iron nucleus is possible. The resulting $\rho(0)$ values, one for the X-ray structure[39] and one for the optimized structure, for **5**, in SNP are given in Table 3.

The correlation between the observed isomer shifts in complexes **1**−**3** and SNP, **5**, and the calculated $\rho(0)$ values is shown in Figure 3, where it is clear that two clusters of points are observed. As expected, the first cluster, with the high isomer shifts and lower $\rho(0)$ values, corresponds to the high-spin iron(II) complexes and the second cluster, with

(49) Böttger, L. H.; Chumakov, A. I.; Grunert, C. M.; Gütlich, P.; Kusz, J.; Paulsen, H.; Ponkratz, U.; Rusanov, V.; Trautwein, A. X.; Wolny, J. A. *Chem. Phys. Lett.* **2006**, *429*, 189–193.

(50) Paulsen, H.; Duelund, L.; Zimmermann, A.; Averseng, F.; Gerdan, M.; Winkler, H.; Toftlund, H.; Trautwein, A. X. *Monatsh. Chem.* **2003**, *134*, 295–306.

(51) Stevens, J. G.; Stevens, V. E. *Mössbauer Effect Data Index*; Plenum: New York, 2006; p 62.

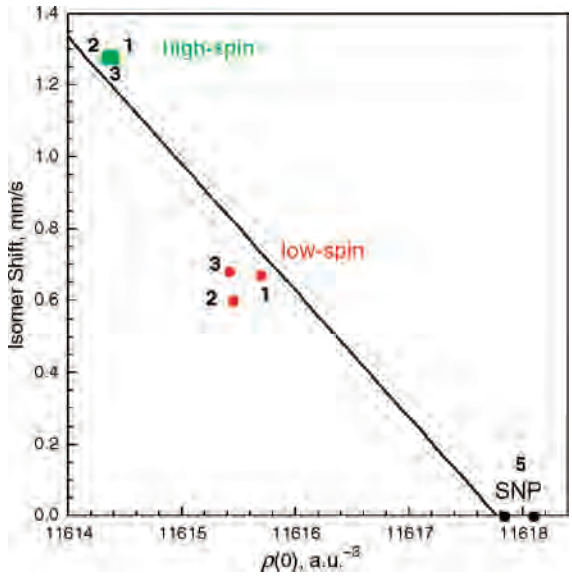

Figure 3. Correlation observed between the observed Mössbauer spectral isomer shifts and $\rho(0)$, the calculated *n*s electron densities at the iron(II) in **1**−**3**. The isomer shifts are given relative to SNP, **5**, and all of the values have been adjusted to 295 K; see Table 3.

lower isomer shifts and higher $\rho(0)$ values, corresponds to the low-spin iron(II) complexes. The solid line in Figure 3 is the result of a linear least-squares fit of all of the data points shown and indicates that a zero isomer shift corresponds to a $\rho(0)$ of 11 617.81 a_0^{-3} for **5** in SNP. The corresponding value for α-iron, which has an isomer shift relative to SNP of 0.2649 mm/s, would be 11 617.06 a_0^{-3}. As is discussed just below, this approach agrees well with the several highly useful methodological approaches developed to relate the observed isomer shift to that of $\rho(0)$ at the iron-57 nucleus.

$$\delta_{SNP} = -0.3534[\rho(0) - 11617.81]\ \text{mm/s} \qquad (2)$$

Some of the observed isomer shifts reported in Table 3 were measured at temperatures other than 295 K. In order to make a comparison between all of the isomer shifts at 295 K, a second-order Doppler shift of -7×10^{-4} (mm/s)/K has been applied to these values.[52] The resulting 295 K values are given in the right-hand column of Table 3, and these values have been used in Figure 3.

A direct comparison of the above relationship with any earlier work is difficult because the exact details of the earlier calculations are often unspecified or the calculations are quite different from those used herein; in some cases, the reference standard is unspecified. Thus, to a first approximation, any comparison between differing functionals and basis sets is difficult and probably of little value for the absolute values of $\rho(0)$. However, we note that the –0.3534 (mm/s)/a_0^{-3} slope found in Figure 3 agrees rather well with the –0.3662 (mm/s)/a_0^{-3} reported by Neese,[36] who also used the B3LYP functional but a different basis set, and is just slightly below the –0.34 to –0.28 (mm/s)/a_0^{-3} range suggested by Nieuwpoort et al.[53] The –0.3534 (mm/s)/a_0^{-3} value is also somewhat less negative than the –0.404 (mm/s)/a_0^{-3} value obtained by Zhang et al.,[18] who also used the B3LYP functional. At this time, it seems that a value close to or even slightly more negative than the –0.34 (mm/s)/a_0^{-3} values suggested earlier[48] may be most suitable. A comparison between the differences in the $\rho(0)$ values obtained for high-spin and low-spin iron(II) ions may also be useful. Herein, we obtain a difference in $\rho(0)$ of ca. 1 a_0^{-3}, whereas a difference of 1.2 a_0^{-3} has been reported[18] for $Fe(phen)_2(NCS)_2$ and a calculated difference of 0.62 a_0^{-3} between high-spin and low-spin $[FeF_6]^{4-}$ has been reported.[53]

Electronic Properties. The energy gaps between the highest occupied molecular orbital (HOMO) and lowest unoccupied molecular orbital (LUMO) of the singlet state of low-spin **1** and for both the α-spin and β-spin orbitals of the high-spin quintet states of **3** and **2** are given in Table S4 in the Supporting Information.

In low-spin **1**, the gap is found to be 5.01 eV for the X-ray structure and the gap increases slightly to 5.25 eV upon structural optimization as the iron(II)-to-ligand bonding distance increases. These very large HOMO–LUMO gap energies are consistent with the expected insulating nature of these complexes. The HOMO and LUMO orbitals for some of the complexes are discussed and shown in the Supporting Information.

Conclusions

In this paper, DFT calculations have been carried out on a family of iron(II) pyrazolylborate complexes that show differing spin-state crossover properties. Because these complexes are neutral, the calculations do not involve any counteranion and hence are fully dependent on the iron(II) nearest-neighbor environment.

We conclude that it is not possible to determine the most stable 0 K iron(II) spin state from the total electronic energies. As has already been observed,[21] and as is indicated by the values given in Table S2 in the Supporting Information, the total 0 K electronic energy is always smaller for the quintet state than for the singlet state in the optimized geometry of the complex after correction for the zero-point vibrational energy.

The sign and the magnitude of the electric field gradient and, hence, the magnitude and sign of the quadrupole splitting at iron(II) for both the high-spin and low-spin states are predicted and reproduced with an accuracy of better than 10% by the B3LYP functional and the various basis sets used herein; see Table S1 in the Supporting Information. Because the calculation of the electron density at the iron nucleus, $\rho(0)$, is not possible with the use of a pseudopotential to model the iron core electrons, a full 6-311++G(d,p) basis set for iron was used to describe all of the iron electrons and calculate $\rho(0)$. These calculations reproduce the large difference in the isomer shift between the high-spin and low-spin states, and a linear correlation between the isomer shift

(52) Shenoy, G. K.; Wagner, F. E.; Kalvius, G. M. In *Mössbauer Isomer Shifts*; Shenoy, G. K., Wagner, F. E., Eds.; North-Holland: Amsterdam, The Netherlands, 1978; pp 49–110.

(53) Nieuwpoort, W. C.; Post, D.; Van Duinen, P. Th. *Phys. Rev. B* **1978**, *17*, 91–98.

and $\rho(0)$ is obtained by using SNP as the Mössbauer-effect iron-57 reference standard.

Acknowledgment. The quantum chemistry computations were carried out at the University of Liège with the support of FRFC9.4545.03F and 1.5187.05 (Belgium). The Ministère de la Région Wallonne is acknowledged for Grant RW/115012.

Supporting Information Available: Basis sets used in the computations (Table S1), calculated total molecular energies (Table S2), X-ray and optimized molecular structures (Table S3), calculated HOMO–LUMO gap energies (Table S4), one of the three approximately degenerate HOMOs of the low-spin singlet state of $Fe[HB(pz)_3]_2$ (Figure S1), one of the three approximately degenerate LUMOs of the low-spin singlet state of $Fe[HB(pz)_3]_2$ (Figure S2), and one of the three approximately degenerate α-spin (a) and β-spin (b) HOMOs of the high-spin quintet state of $Fe[HB(3\text{-}Mepz)_3]_2$ (Figure S3). This material is available free of charge via the Internet at http://pubs.acs.org.

IC701367B